Solid State Electronics 147 (2018) 39–43

Contents lists available at ScienceDirect

Solid State Electronics

journal homepage: www.elsevier.com/locate/sse

Lumped-element model of plasmonic solar cells

Chang-Hyun Kim[a,b,*], Maria Seitanidou[c], Jong Woo Jin[a], Yvan Bonnassieux[a], Gilles Horowitz[a], Ioannis Vangelidis[d], Elefterios Lidorikis[d], Argiris Laskarakis[c], Stergios Logothetidis[c]

[a] LPICM, Ecole Polytechnique, CNRS, 91128 Palaiseau, France
[b] Department of Electronic Engineering, Gachon University, Seongnam 13120, Republic of Korea
[c] Laboratory for Thin Films-Nanosystems and Nanotechnology, Department of Physics, Aristotle University of Thessaloniki, Thessaloniki 54124, Greece
[d] Department of Materials Science and Engineering, University of Ioannina, Ioannina 45110, Greece

ARTICLE INFO

The review of this paper was arranged by Y. Kuk

Keywords:
Equivalent circuits
Lumped-element model
Metal nanoparticles
Plasmonics
Solar cells

ABSTRACT

Although metallic nanostructures in solar cells provide versatility in designing useful plasmonic architectures, understanding is still limited on how to exploit their multi-scale contribution as tunable performance. In this article, we suggest a characteristic model that develops into a simple and robust tool for guiding optimization of plasmonic solar devices. The model is conceptually based on the breakdown of the active region into intrinsic and plasmonic sub-circuits, by which the terminal currents are directly correlated with particle geometries and local improvement. Measurements from organic cells support the validity of our theory, and a series of simulation provides further insights into the critical trade-off between voltage and current generation, finally offering a strategy for efficiency enhancement.

1. Introduction

The field of nanotechnology relies on synthesis and control of nanoscale objects that are engineered to undertake active functions in higher-level architectures [1,2]. Therefore, challenges remain on making structures, processes, and interfaces that produce meaningful improvement when embedding nanomaterials into device platforms. Such argument merits special consideration for discussing systems such as plasmonic solar cells [3]. In principle, collective oscillation of electrons in metallic nanostructures dictates substantial amplification of excitation field [4]. However, these effects are strongly localized in nature, and absorption enhancement seen at the device level has been often moderate or highly structure and processing dependent [5,6]. Furthermore, excess metal-semiconductor junctions at plasmonic interfaces are likely to make it harder to extract the maximum of benefits because of simultaneous increase in recombination and quenching losses [7].

Lumped-element modeling is a promising technique to collectively take into account optical, electrical, and structural aspects of plasmonics, providing a means of rational optimization of solar cells [8]. As physical processes are packed into circuit elements, the device operation can be readily visualized to manifest the impact of phenomena on macroscopic measurables (e.g. terminal currents). Also, such a model can serve as a bridge in multi-scale investigation because on one hand, microscopic insights can be obtained through correlation with atomic/molecular-level theories, and on the other hand, larger-scale systems can be predicted by connecting a multitude of cells with necessary components [9]. Equivalent circuits have been previously employed for related topics, proving their powerfulness in tackling diverse scientific questions. Examples include the study of non-ideality in organic solar cells [10], characteristics of nanoplasmonic antennas [11], size effects of perovskite solar cells [12], and single-cell approximation of photovoltaic modules [13].

In this article, we formulate a lumped-element model for the solar cells that include metal nanoparticles (NPs). To pinpoint critical factors affecting plasmonic enhancement, we investigate various sources of positive and negative effects of having NPs in core structures. We first take an inverse modeling approach to reproduce the trends in experimental observations [14], and proceed to simulate hidden aspects of cell behaviors by systematically scanning several parametric dimensions.

2. Experimental methods

Test devices were fabricated using organic semiconductor materials. Clearly, plasmonics brings the possibility of reducing the thickness of semiconductor necessary for light absorption [15], and this implies an economic impact. As one of the organic electronics' targets is low-cost products using roll-to-roll fabrication [16], exploitation of plasmonic effects is in line with the promise of this field. Our devices were

* Corresponding author at: Department of Electronic Engineering, Gachon University, Seongnam 13120, Republic of Korea.
E-mail address: chang-hyun.kim@gachon.ac.kr (C.-H. Kim).

https://doi.org/10.1016/j.sse.2018.06.005
Received 1 December 2017; Received in revised form 27 March 2018; Accepted 8 June 2018
Available online 13 June 2018
0038-1101/

fabricated inside a nitrogen-filled glove box. Anode indium tin oxide (ITO)-coated glass slides were first cleaned by ultrasonication in deionized water, acetone, isopropanol and methanol, and dried on a hot plate. Then, poly(3,4-ethylenedioxythiophene) poly(styrenesulfonate) (PEDOT:PSS) films were deposited by spin coating at 4000 rpm for 30 s onto the substrates and dried on a hot plate at 145 °C for 10 min. Ag NPs were formed by the polyol method [17]. Depending on the target structure, the NPs were spin-coated either on the PEDOT:PSS layer or on the active layer, followed by annealing at 145 °C for solvent evaporation. The active layer was made of the bulkheterojunction of regioregular poly(3-hexylthiophene) (P3HT) (purity of 99.995%) and (6,6)-phenyl C61 butyric acid methyl ester (PCBM) (purity of 99.5%), an architypal system in the organic solar cell technology [18]. The solution of P3HT:PCBM (1:0.8 in weight) was prepared at a total concentration of 50 mg/ml in 1,2-dichlorobenzene. The solution was stirred for over 24 h at 65 °C. The blend was then spin-coated at 1000 rpm for 30 s onto the PEDOT:PSS layer. The devices were finalized by thermal evaporation of the Ca/Al cathode.

3. Results and discussion

3.1. Structural description

The X-ray diffraction (XRD) pattern of Fig. 1(a) indicates that our NPs are geometrically well defined with crystallinity, a remarkable property for solution-processed materials. Also shown in Fig. 1(a) is the atomic-force microscope (AFM) image that visualizes surface distribution of these spin-cast Ag NPs. An approximation is introduced for a uniform two-dimensional (2-D) array of circular islands, as depicted in Fig. 1(b) (top view). Here, l is the diameter of an NP, a is the lattice constant of the unit cell (equivalent to the inter-particle distance), and A is the total active area of a solar cell. This parametrization leads to the definition of several auxiliary values; the single-particle area as $\pi(l/2)^2$, the number of unit cells (= the number of NPs) in the total active area as A/a^2, and the total area occupied by the NPs as $A\pi(l/2a)^2$.

3.2. Current-voltage relationship

Our idea for modeling a solar cell is to consider the current path in the active volume as a network of characteristic impedances. As shown in Fig. 2(a), Z_{int} and Z_{np} correspond to the unit-area impedance of an intrinsic zone and that of an NP zone, respectively. The opto-electronic functionalities in these two regions are supposed to differ substantially, and therefore we regard each region as an effective sub-cell and assign equivalent circuits with independent parameters as shown in Fig. 2(b) and (c) [19]. The current-voltage relationships for these sub-structures are deduced as

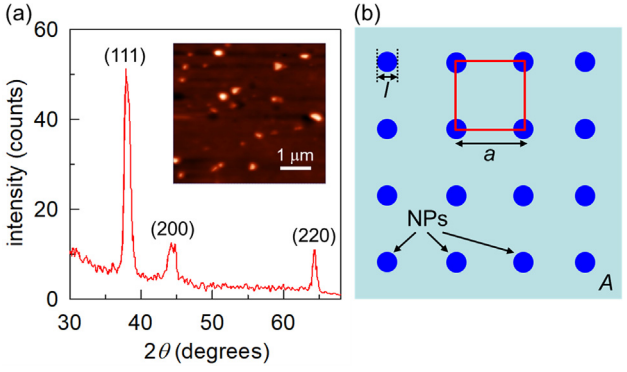

Fig. 1. (a) XRD pattern measured on the Ag NPs deposited on a glass substrate (inset: AFM image of the solution-processed Ag NP arrays). (b) Schematic illustration that parametrizes the two-dimensional spatial distribution of NPs.

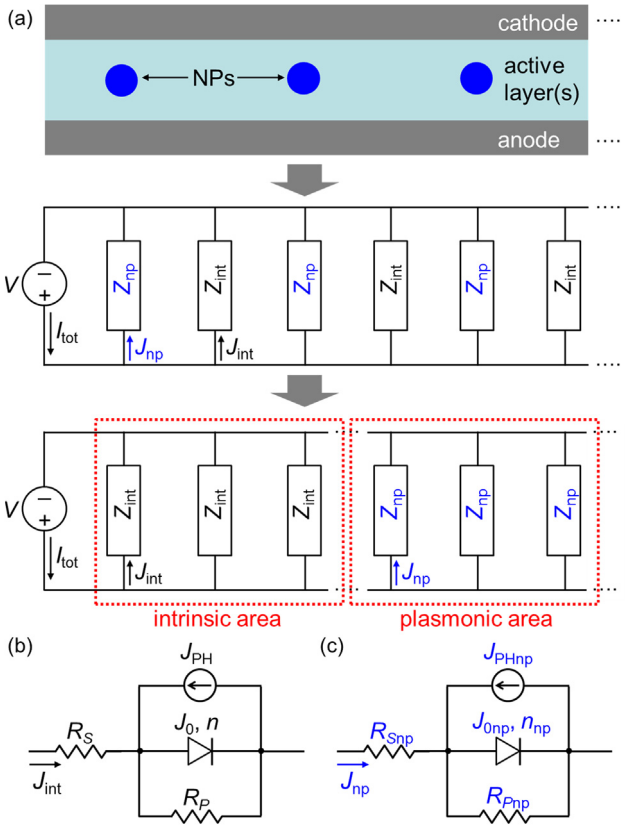

Fig. 2. (a) Description of the lumped-element model. Top: Simplified cross-sectional structure of a solar cell. Middle: Assignment of the intrinsic and plasmonic impedance to the corresponding areas. Bottom: Re-arrangement of parallel branches to sum up the contributions within each characteristic zone. (b) Sub-circuit structure of Z_{int}. (c) Sub-circuit structure of Z_{np}.

$$J_{int} = J_0\left[\exp\left\{\frac{q(V-J_{int}R_S)}{nkT}\right\}-1\right] + \frac{V-J_{int}R_S}{R_P} - J_{PH}, \quad (1)$$

and

$$J_{np} = J_{0np}\left[\exp\left\{\frac{q(V-J_{np}R_{Snp})}{n_{np}kT}\right\}-1\right] + \frac{V-J_{np}R_{Snp}}{R_{Pnp}} - J_{PHnp}. \quad (2)$$

Here, J_{int} is the current density of an intrinsic sub-circuit, with J_0 as the diode saturation current density, n as the diode ideality factor, R_S as the area-multiplied series resistance, R_P as the area-multiplied parallel resistance, and J_{PH} as the photocurrent density. The parameters in Eq. (2) are the counterparts for a plasmonic sub-circuit. As the constituent branches are connected in parallel, they can be re-arranged as two groups [Fig. 2(a) bottom], from which the total current I_{tot} can be constructed as the area-weighted sum of intrinsic and plasmonic current densities. From the notations of Fig. 1, this expression translates into

$$\begin{aligned} I_{tot} &= I_{int} + I_{np} \\ &= J_{int}A\left\{1-\pi\left(\frac{l}{2a}\right)^2\right\} + J_{np}A\pi\left(\frac{l}{2a}\right)^2, \end{aligned} \quad (3)$$

and finally, the total current density J_{tot} is given as

$$J_{tot} = \frac{I_{tot}}{A} = J_{int}\left\{1-\pi\left(\frac{l}{2a}\right)^2\right\} + J_{np}\pi\left(\frac{l}{2a}\right)^2. \quad (4)$$

3.3. Application to real devices

A major feature of our method is the ability to access the pure traits

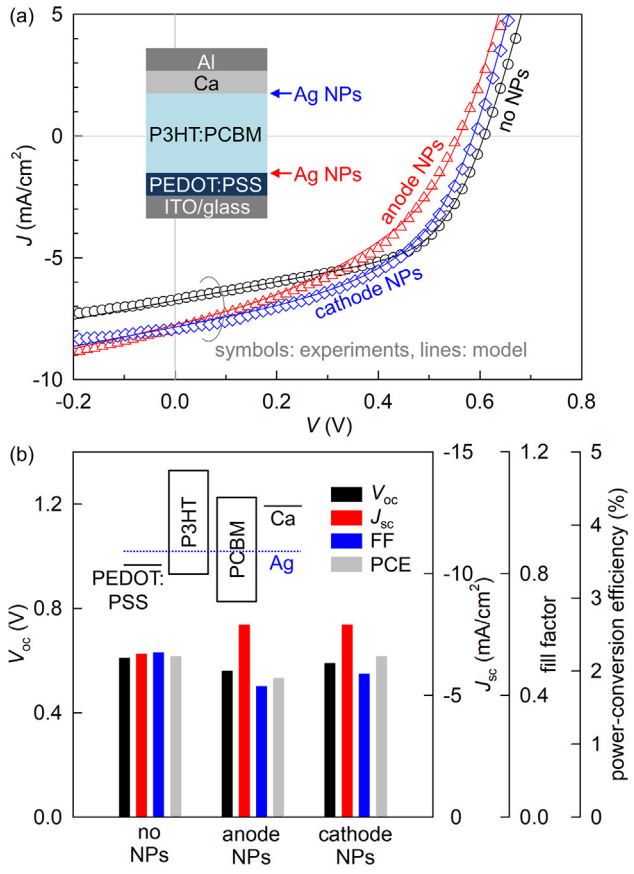

Fig. 3. (a) Comparison between the measured (symbols) and modeled (lines) *J-V* curves from an intrinsic cell and two NP-incorporating plasmonic cells. Inset: Structure of the fabricated P3HT:PCBM devices. (b) Solar cell parameters extracted from the experimental *J-V* characteristics. Inset: Energy diagram of the key materials affecting the level alignment around the photo-active region.

of plasmonic components inside a cell in reference to an entirely intrinsic device. As an example, we applied the model to the three devices depicted in Fig. 3(a); a cell without NPs and two plasmonic cells with Ag NPs at the anode or cathode side. We first set $l = 0$ in Eq. (4) to yield $J_{tot} = J_{int}$, and fit the data from the intrinsic cell to Eq. (1). As shown in Fig. 3(a), the overall behavior is well described by this equation, with the parameters determined as $J_0 = 7.0 \times 10^{-10}$ A/cm^2, $n = 1.5$, $R_S = 9.0$ Ω·cm^2, $R_P = 250$ Ω·cm^2, $J_{PH} = 7.0$ mA/cm^2. Next, the geometrical parameter was deduced from the AFM analysis as $l/a = 0.2$. Now that the values of J_{int} and l/a are given, we can fit the data from the plasmonic cells to Eq. (4) to get J_{np} and its sub-circuit parameters. Fig. 3(a) shows that the measured currents of both plasmonic devices are in excellent agreement with the model. Here, $J_{0np} = 5.0 \times 10^{-4}$ A/cm^2, $n_{np} = 3.0$, $R_{Snp} = 2.0$ Ω·cm^2, $R_{Pnp} = 30$ Ω·cm^2, $J_{PHnp} = 42$ mA/cm^2 for the anode-NP sample, and $J_{0np} = 1.0 \times 10^{-4}$ A/cm^2, $n_{np} = 3.0$, $R_{Snp} = 2.0$ Ω·cm^2, $R_{Pnp} = 160$ Ω·cm^2, $J_{PHnp} = 42$ mA/cm^2 for the cathode-NP sample.

Basic solar-cell parameters are summarized in Fig. 3(b). There is a substantial increase in short-circuit current density (J_{sc}) in the NP-incorporating cells, benefiting from plasmonic near-field enhanced absorption [20]. However, the open-circuit voltage (V_{oc}) and fill factor (FF) decreased somewhat, leading to a power-conversion efficiency (PCE) either slightly lower than or on a par with that of the reference cell. Such clearly counteracting outcomes of NPs are well resolved in our model and the circuit elements therein. The noticeably high value found for J_{PHnp} ($\gg J_{PH}$) is a main source of enhancement for J_{sc}. However, the values of the majority of the other parameters deteriorated from the values of their intrinsic counterparts ($J_{0np} > J_0$, $n_{np} > n$, and $R_{Pnp} < R_P$). This is interpreted as pronounced electrical imperfections in rectification and current driving of the NP regions of a cell [21–23]; hence, despite the obvious optical advantages, these effects become a major cause of reduction in V_{oc} and FF. The evolution of series resistance ($R_{Snp} < R_S$) is regarded as the result of reduced bulk resistivity with metal contents, which is shown to have minor effects on the high positive voltage regime.

When comparing the two plasmonic devices, the position of NPs is mainly reflected on V_{oc}. We infer that Ag NPs in intimate contact with PEDOT:PSS can reduce the effective work function of the anode, resulting in a smaller V_{oc} (Fig. 3(b) inset) [24]. In contrast, the majority of electrons flowing from PCBM are likely to be captured by Ca, which has large contact areas with the Fermi level energetically close to the lowest-unoccupied molecular orbital of PCBM, thus having a minimal impact on V_{oc} [25].

3.4. Parameter variation

Using the validated model as a tool, we can project the performance of devices by predictive simulations [7,14]. The discussion for Fig. 3 showed limitations in plasmonic enhancement associated with the interplay between physical mechanisms. In this regard, we took the extracted parameter set of the cathode-NP solar cell, and conducted systematic simulations by changing the value of l/a, an important factor dictating the spatial occupation of NPs. The results are given in Fig. 4, showing that calculated J_{tot} gradually approaches J_{np} as l/a varies from 0.1 to 1.0. The V_{oc} and J_{sc} are estimated for each curve, and plotted against l/a in the inset. Here, we observe a clearly reverse trend in variation of these two key performance metrics, evidencing a critical trade-off between photo-induced voltage and current. Furthermore, it implies that there can be a potential optimum in particle size and distribution for maximizing the PCE of a plasmonic cell, even though the cell efficiency monotonously increases with l/a in this particular simulation due to the dominant effect of current enhancement. We also note here that J_{tot} with $l/a = 1.0$ does not overlap with J_{np} because this condition forces the NPs to touch each other leaving an empty space at the center of unit cell (Fig. 1(b)).

Finally, we carried out focused simulations to find a strategy for designing a solar cell with higher PCEs. Our analysis of the fabricated devices indicates that electrical leakage in the low-voltage regime of the diode is a major factor in suppressing the PCE improvement, which seems to be a downside of adding nanoscale conductors [23]. To

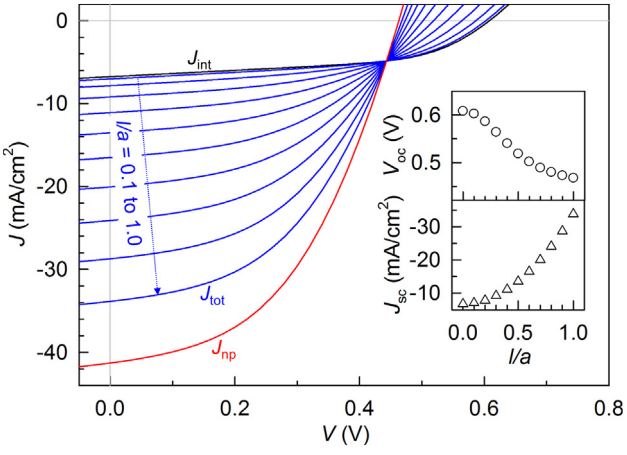

Fig. 4. Results of a series of simulation that visualizes the direct impact of geometrical occupation l/a on the performance of a solar cell. Black and red solid lines correspond to J_{int} and J_{np}, respectively, while J_{tot} is represented by the group of blue solid lines that are calculated with different l/a values. Inset: Extracted V_{oc} and J_{sc} as a function of l/a. (For interpretation of the references to colour in this figure legend, the reader is referred to the web version of this article.)

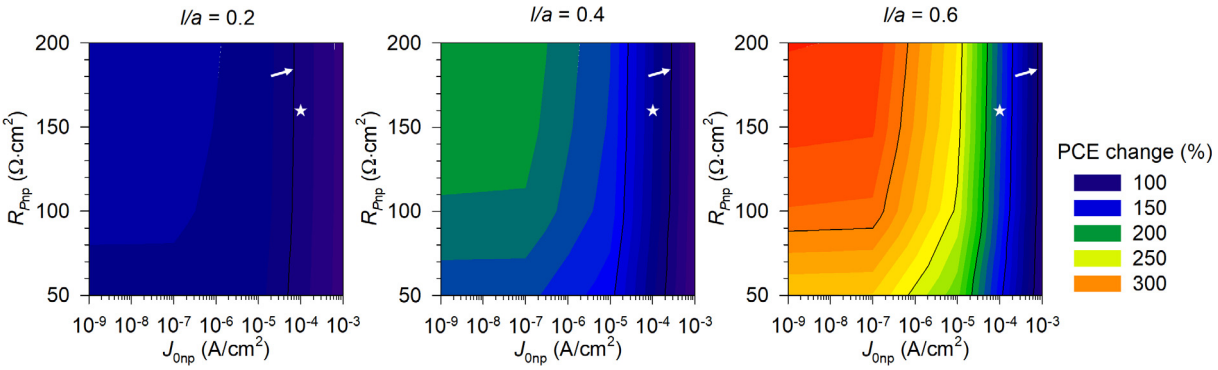

Fig. 5. Prediction of the PCE change with varying plasmonic parameters J_{0np} and R_{Pnp}. Each panel assumes a fixed l/a of 0.2 (left), 0.4 (middle), and 0.6 (right). All of the black solid lines in the contour plots are placed at 50% intervals, with the 100% line in each plot being marked by a white arrow. In addition, the reference point corresponding to the parameters extracted from the cathode-NP device is shown as a white star in each plot.

address this issue, we deliberately increased the R_{Pnp} and decreased J_{0np} from the levels seen at our plasmonic cells, both of which meaning the direction of mitigating leakage transport [26,27]. Within a fixed 2-D parameter space, the PCE change was calculated as the ratio of the PCE of the plasmonic cell to that of the intrinsic cell, and this analysis was extended to three different geometries as shown in Fig. 5. Therefore, the 100% contours, pointed out by the white arrows, demarcate a net decrease and increase in PCE from inclusion of NPs. Here, a zone under this border line appears in all cases, reaffirming the fact that net enhancement of PCE is not guaranteed. Decrease in J_{0np} and increase in R_{Pnp} is shown to endow a cell with significant PCE enhancement, with overall improvement in the case of large l/a. Although envisioning promising performance in optimized devices, this result indicates that a large J_{0np} is particularly problematic, degrading the PCE to the level even below that of the intrinsic cell. To overcome the limitation, several guidelines can be proposed. Above all, suppressing leakage currents while maintaining high NP population becomes both a major challenge and a key strategy. A geometrical current, such as fringing conduction and in-metal transport, is supposed to be a major origin of low parallel resistance [26,28]. Therefore, patterning and isolation of NPs can be an effective way to maximize R_{Pnp}, and core-shell particle structures with oxide encapsulation may also serve the same purpose [29,30]. On the other hand, the saturation current of a rectifying diode is mostly affected by energy level alignments [23]. From this aspect, the metal forming NPs should be chosen in consideration of frontier levels of surrounding materials, and surface engineering using self-assembled monolayers can be a promising route to a lowered J_{0np} through optimized interface chemistry and controlled charge-carrier dynamics [31]. While it was not taken as a variable for calculations in Fig. 5, n_{np} is also an important parameter to minimize for overall device improvement. It was revealed that carrier recombination/exciton quenching at metal-organic interfaces and Gaussian energetic disorder can significantly increase the ideality factor [32,33]. Therefore, the above-proposed NP functionalization methods should also help reduce this parameter, and novel hybridization techniques such as blending with an insulating polymer may also enhance the cell performance by suppressing the disorder-limited transport [34].

4. Conclusion

We have developed an effective approach to model the behavior of nano-plasmonic solar cells based on lumped-element principles. Our treatment has simplified the use of circuit theories to solve the current-voltage characteristics of practical NP-containing devices. As the suggested method allows one to precisely fit the given experimental data and readily simulate unexplored dimensions, we expect that it can be widely employed to analyze and optimize promising next-generation plasmonic solar cells and related nano-hybrid architectures.

Acknowledgments

This work was supported by the European Union Seventh Framework Program (FP7/2007-2013) under grant agreement number 310229 (SMARTONICS).

References

[1] Reed MA, Lee T, editors. Molecular nanoelectronics. Stevenson Ranch, CA: American Scientific Publishers; 2003.
[2] Natelson D. Nanostructures and nanotechnology. Cambridge: Cambridge University Press; 2015.
[3] Atwater HA, Polman A. Plasmonics for improved photovoltaic devices. Nat Mater 2010;9:205–13.
[4] Lidorikis E. Modeling of enhanced absorption and Raman scattering caused by plasmonic nanoparticle near fields. J Quant Spectrosc Radiat Transf 2012;113:2573–84.
[5] Kalfagiannis N, Karagiannidis PG, Pitsalidis C, Panagiotopoulos NT, Gravalidis C, Kassavetis S, et al. Plasmonic silver nanoparticles for improved organic solar cells. Sol Energy Mater Sol Cells 2012;104:165–74.
[6] Beliatis MJ, Henley SJ, Han S, Gandhi K, Adikaari AADT, Stratakis E, et al. Organic solar cells with plasmonic layers formed by laser nanofabrication. Phys Chem Chem Phys 2013;15:8237–44.
[7] Kim C-H, Choi J, Bonnassieux Y, Horowitz G. Simplified numerical simulation of organic photovoltaic devices. J Comput Electron 2016;15:1095–102.
[8] Senturia SD. Microsystem design. New York, NY: Springer; 2005.
[9] Maneux C, Fregonese S, Zimmer T, Retailleau S, Nguyen HN, Querlioz D, et al. Multiscale simulation of carbon nanotube transistors. Solid-State Electron 2013;89:26–67.
[10] García-Sánchez FJ, Lugo-Muñoz D, Muci J, Ortiz-Conde A. Lumped parameter modeling of organic solar cells' s-shaped I−V characteristics. IEEE J Photovolt 2013;3:330–5.
[11] Choi Y, Choi D, Lee LP. Metal−insulator−metal optical nanoantenna with equivalent-circuit analysis. Adv Mater 2010;22:1754–8.
[12] Lin Q, Nagiri RCR, Burn PL, Meredith P. Considerations for upscaling of organo-halide perovskite solar cells. Adv Opt Mater 2017;5:1600819.
[13] Kim C-H, Beliatis MJ, Gandhi KK, Rozanski LJ, Bonnassieux Y, Horowitz G, et al. Equivalent circuit modeling for a high-performance large-area organic photovoltaic module. IEEE J Photovolt 2015;5:1100–5.
[14] Kim C-H, Hlaing H, Kymissis I. A macroscopic model for vertical graphene-organic semiconductor heterojunction field-effect transistors. Org Electron 2016;36:45–9.
[15] Hayashi S, Okamoto T. Plasmonics: visit the past to know the future. J Phys D: Appl Phys 2012;45:433001.
[16] Krebs FC, Tromholt T, Jørgensen M. Upscaling of polymer solar cell fabrication using full roll-to-roll processing. Nanoscale 2010;2:873–86.
[17] Kim D, Jeong S, Moon J. Synthesis of silver nanoparticles using the polyol process and the influence of precursor injection. Nanotechnology 2006;17:4019–24.
[18] Trung Dang M, Hirsch L, Wantz G. P3HT:PCBM, best seller in polymer photovoltaic research. Adv Mater 2011;23:3597–602.
[19] Kippelen B, Brédas J-L. Organic photovoltaics. Energy Environ Sci 2009;2:251–61.
[20] Lagos N, Sigalas MM, Lidorikis E. Theory of plasmonic near-field enhanced absorption in solar cells. Appl Phys Lett 2011;99:063304.
[21] Pallarès J, Cabré R, Marsal LF, Schropp REI. A compact equivalent circuit for the dark current-voltage characteristics of nonideal solar cells. J Appl Phys 2006;100:084513.
[22] Wetzelaer GAH, Koster LJA, Blom PWM. Validity of the Einstein relation in disordered organic semiconductors. Phys Rev Lett 2011;107:066605.
[23] Kim CH, Yaghmazadeh O, Bonnassieux Y, Horowitz G. Modeling the low-voltage regime of organic diodes: origin of the ideality factor. J Appl Phys 2011;110:093722.

[24] Qi B, Wang J. Open-circuit voltage in organic solar cells. J Mater Chem 2012;22:24315–25.
[25] Guan Z-L, Kim JB, Wang H, Jaye C, Fischer DA, Loo Y-L, et al. Direct determination of the electronic structure of the poly(3-hexylthiophene):phenyl-[6,6]-C61 butyric acid methyl ester blend. Org Electron 2010;11:1779–85.
[26] van Mensfoort SLM, Shabro V, de Vries RJ, Janssen RAJ, Coehoorn R. Hole transport in the organic small molecule material α-NPD: evidence for the presence of correlated disorder. J Appl Phys 2010;107:113710.
[27] Hlaing H, Kim C-H, Carta F, Nam C-Y, Barton RA, Petrone N, et al. Low-voltage organic electronics based on a gate-tunable injection barrier in vertical graphene-organic semiconductor heterostructures. Nano Lett 2015;15:69–74.
[28] Kim C-H, Hlaing H, Yang S, Bonnassieux Y, Horowitz G, Kymissis I. Impedance spectroscopy on copper phthalocyanine diodes with surface-induced molecular orientation. Org Electron 2014;15:1724–30.
[29] Akimov YA, Koh WS. Resonant and nonresonant plasmonic nanoparticle enhancement for thin-film silicon solar cells. Nanotechnology 2010;21:235201.
[30] Brown MD, Suteewong T, Kumar RSS, D'Innocenzo V, Petrozza A, Lee MM, et al. Plasmonic dye-sensitized solar cells using core−shell metal−insulator nanoparticles. Nano Lett 2011;11:438–45.
[31] Miozzo L, Yassar A, Horowitz G. Surface engineering for high performance organic electronic devices: the chemical approach. J Mater Chem 2010;20:2513–38.
[32] Street RA, Schoendorf M, Roy A, Lee JH. Interface state recombination in organic solar cells. Phys Rev B 2010;81:205307.
[33] Garcia-Belmonte G. Carrier recombination flux in bulk heterojunction polymer:fullerene solar cells: effect of energy disorder on ideality factor. Solid-State Electron 2013;79:201–5.
[34] Yu K, Park B, Kim G, Kim C-H, Park S, Kim J, et al. Optically transparent semiconducting polymer nanonetwork for flexible and transparent electronics. Proc Natl Acad Sci USA 2016;113:14261–6.

Chang-Hyun Kim is an Assistant Professor of Electronic Engineering at Gachon University, Republic of Korea. His research focuses on the development of novel electronic devices based on organic semiconductors and hybrid nanoarchitectures. After receiving a Ph.D. in physics from the Ecole Polytechnique, France, he worked at Columbia University, the French National Centre for Scientific Research (CNRS), and Gwangju Institute of Science and Technology (GIST). Prof. Kim was a recipient of the Alliance Doctoral Mobility Award, the Prix de thèse (Ph.D. thesis award) of the Ecole Polytechnique, and the Korean Ministry of Education Research Fellowship.